UV-Vis/FT-NIR in situ monitoring of visible-light induced polymerization of PEGDA hydrogels initiated by eosin/triethanolamine/O_2

Citation: Kaastrup, Kaja; Aguirre-Soto, Alan; Wang, Chen; Bowman, Christopher N.; Stansbury, Jeffrey W. and Sikes, Hadley D. "UV-Vis/FT-NIR in Situ Monitoring of Visible-Light Induced Polymerization of PEGDA Hydrogels Initiated by eosin/triethanolamine/O_2." Polymer Chemistry 7, no. 3 (January 2016): 592–602 © 2016 The Royal Society of Chemistry

As Published: http://dx.doi.org/10.1039/c5py01528f

Publisher: Royal Society of Chemistry, The

Persistent URL: http://hdl.handle.net/1721.1/109788

Version: Author's final manuscript: final author's manuscript post peer review, without publisher's formatting or copy editing

HHS Public Access

Author manuscript

Polym Chem. Author manuscript; available in PMC 2017 January 01.

Published in final edited form as:

Polym Chem. 2016 ; 7(3): 592–602. doi:10.1039/C5PY01528F.

UV-Vis/FT-NIR *in situ* monitoring of visible-light induced polymerization of PEGDA hydrogels initiated by eosin/triethanolamine/O_2

Kaja Kaastrup[a], **Alan Aguirre-Soto**[a,b], **Chen Wang**[b], **Christopher N. Bowman**[b], **Jeffery Stansbury**[b,c], and **Hadley D. Sikes**[a,d,*]

[a]Department of Chemical Engineering, Massachusetts Institute of Technology, Cambridge, MA 02139, United States

[b]Department of Chemical and Biological Engineering, University of Colorado Boulder, 3415 Colorado Ave., Boulder, Colorado 80303, United States

[c]Department of Craniofacial Biology, School of Dental Medicine, University of Colorado, 12800 East 19th Ave., Aurora, Colorado 80045, United States

[d]Program in Polymers and Soft Materials, Massachusetts Institute of Technology, Cambridge, MA, 02139, United States

Abstract

In conjunction with a tertiary amine coinitiator, eosin, a photoreducible dye, has been shown to successfully circumvent oxygen inhibition in radical photopolymerization reactions. However, the role of O_2 in the initiation and polymerization processes remains inconclusive. Here, we employ a UV-Vis/FT-NIR analytical tool for real-time, simultaneous monitoring of chromophore and monomer reactive group concentrations to investigate the eosin-activated photopolymerization of PEGDA-based hydrogels under ambient conditions. First, we address the challenges associated with spectroscopic monitoring of the polymerization of hydrogels using UV-Vis and FT-NIR, proposing metrics for quantifying the extent of signal loss from reflection and scattering, and showing their relation to microgelation and network formation. Second, having established a method for extracting kinetic information by eliminating the effects of changing refractive index and scattering, the coupled UV-Vis/FT-NIR system is applied to the study of eosin-activated photopolymerization of PEGDA in the presence of O_2. Analysis of the inhibition time, rate of polymerization, and rate of eosin consumption under ambient and purged conditions indicates that regeneration of eosin in the presence of oxygen and consumption of oxygen occur via a nonchain process. This suggests that the uniquely high O_2 resilience is due to alternative processes such as energy transfer from photo-activated eosin to oxygen. Uncovering the intricacies of the role of O_2 in eosin-mediated initiation aids the design of O_2 resistant free radical polymerization systems relevant to photonics, optoelectronics, biomaterials, and biosensing.

*Correspondence: sikes@mit.edu.

Electronic Supplementary Information (ESI) Available: See DOI: 10.1039/x0xx00000x

Keywords

UV-Vis; Near Infrared; Spectroscopy; Hydrogels; Photopolymerization; Oxygen inhibition

Introduction

Free radical, light-induced polymerization reactions are an essential and commonly used tool in a wide range of industries including microelectronics, laser imaging, and the production of coatings and adhesives.[1,2] Photopolymerization offers advantages in comparison with alternative methods such as thermal or redox initiation, including short reaction times, ambient reaction temperatures, and spatial and temporal control.[2] As a result, increasingly diverse reactions have been developed to initiate polymerization reactions with light. Visible-light initiation, in particular, has attracted significant interest because of growth in the fields of biomaterials and electronics, where initiation using UV light is sometimes undesirable or impractical. Rational design of improved systems for visible-light initiation is challenging since the identification of key criteria depends on the elucidation of often-complex mechanisms. We apply coupled UV-Vis/FT-NIR real-time spectroscopy towards the elucidation of the mechanistic complexities of the light-induced, chain-growth polymerization of poly(ethylene glycol) diacrylate (PEGDA) hydrogels initiated by eosin in the presence of triethanolamine (TEA) and oxygen. This chemistry has been used in a variety of applications, including lithography,[3] 3D printing,[4] biomaterials,[5,6] and biosensing.[7–9]

Eosin/amine formulations have been shown to initiate polymerization in spite of a 1000-fold excess of oxygen.[10] However, the mechanism through which eosin is able to overcome large excess O_2 concentrations is controversial. The mechanism of oxygen inhibition when using typical photocleaving chromophores is well known; O_2 reacts with initiating and propagating radicals to produce peroxy radicals that are relatively unreactive towards the monomer vinyl groups,[11,12] and, thus, have the effect of terminating the reaction. Solutions to O_2 inhibition include purging with inert gases, adding antioxidants and oxygen sensitizers (molecules that transfer their triplet energy to triplet oxygen), or adding hydrogen donors (amines, cyclic N-vinylamides, thiols) to promote chain peroxidation through which reactive radicals are regenerated from peroxy radicals.[12] The mechanism of oxygen inhibition with non-cleaving chromophores is more complex than that of photocleaving chromophores because of the competition between an increased number of photochemical and photophysical reaction pathways. A possible route through which eosin is regenerated via hydrogen abstraction by peroxy radicals from the semiquinone form of eosin ($EH^{\cdot}$) has been proposed.[10,13] However, recent theoretical evidence suggests that despite its kinetic feasibility, this reaction alone appears insufficient to explain eosin's extraordinary resistance to excess O_2.[14]

Spectroscopic techniques enable the measurement of reaction kinetics by providing the ability to track the absorbance of light by reactants a function of time as a polymerization reaction proceeds. An early approach to monitoring polymerization kinetics was to take discrete, periodic measurements of a reaction mixture.[15] Real-time monitoring of

polymerization, and particularly monomer conversion using FTIR, has since become routine.[16,17] In the UV-visible range, absorbance and fluorescence spectroscopy have been employed previously to investigate initiator (dye) regeneration. Slower rates of absorbance and fluorescence decay have been associated with regeneration.[18,19] *In situ* UV-Vis and FT-IR spectroscopy have been used separately to monitor the copolymerization of furan and thiophene; UV-Vis spectra were used to determine the relative incorporation of thiophene and furan into the polymer based on the characteristic absorption bands of polyfuran and polythiophene.[20] Decker performed separate measurements with real-time UV-Vis and IR spectroscopy to study the kinetics of UV-initiator photolysis and polymerization, respectively.[21]

In some systems, light also interacts with the polymer product via non-absorptive processes so that optical measurements contain additional information related to polymer structure.[22–26] UV-Vis spectroscopy has been used to measure photoinitiator consumption and track changes in refractive index during polymerization reactions.[27] Kang et al. presented a method for determining the chemical cross-link density in real time using UV-Vis spectroscopy.[28] Reed and colleagues developed an online technique for monitoring molar mass during polymerization reactions that operates through the continuous withdrawal of a small stream of sample that is diluted with solvent and routed through light scattering, refractometry and viscometry detectors in series.[29,30]

Recently, Aguirre-Soto et al. demonstrated a custom coupled UV-Vis/FT-NIR apparatus (Fig. 1) that permits simultaneous monitoring of the concentrations of the absorbing initiator and the monomer reactive groups *in situ* without the need for sample extraction.[31] This dual monitoring technique was used to study the polymerization of bulk methacrylate monomers initiated by camphorquinone and amine. In this system, spectral changes were solely due to electronic and vibrational transitions without contributions from non-absorptive processes.

Here, we employ dual UV-Vis/FT-NIR monitoring to examine the role of oxygen in a radical polymerization reaction by quantifying the eosin concentration using its π-π* transition and the monomer vinyl group conversion using the vinyl group NIR overtone band (Fig. 1b and c). Previous studies have been limited to monitoring either double bond conversion[10] or photoinitiator consumption[13] in examining the role of oxygen in this hydrogel-forming reaction. The advantage of using a set-up that allows for simultaneous monitoring of the chromophore consumption and the monomer conversion is that it becomes possible to measure how the chromophore is consumed specifically during the inhibition period. In order to achieve this goal, it was necessary to address the challenge of signal loss due to optical attenuation from time-dependent refraction and scattering of the UV-Vis probing beam (i.e. non-absorptive processes). We present a signal deconvolution strategy for quantifying the optical attenuation and eosin's absorbance. We then analyze the data to determine the duration of the inhibition period, the rates of eosin consumption in different stages of the reaction, and the rate of polymerization. Furthermore, we show for the first time how UV-Vis attenuation kinetics provide information about the formation of hydrophobic PEGDA-rich microgels, heterogeneities, and swelling during the hydrogel polymerization.

Experimental section

Materials

Poly(ethylene glycol) diacrylate (average M_n 575), triethanolamine (TEA), 1-vinyl-2-pyrrolidone (VP), and 2′,4′,5′,7′-tetrabromofluorescein disodium salt (eosin Y; E) were purchased from Sigma Aldrich. Distilled water was used.

Preparation of monomer solutions

Monomer solutions were prepared with 420 mM PEGDA, 35 mM VP, 210 mM TEA, and 5 μM eosin Y in DI water (equivalent to 21.6% PEGDA, 2.8% TEA, 0.4% VP, 75.2% water by volume). In the case of the purged samples, argon was bubbled through the solution for 5 minutes prior to transfer to the cuvettes for polymerization. These samples were polymerized under Nitrogen flow (8 psi). Between three and five replicates were performed at each condition.

Coupled UV-Vis and FT-NIR monitoring set-up

Dual pathlength (10 × 2 mm) PMMA cuvettes (UVette, Eppendorf, Hauppauge, NY) with transmission in the 220–1600 nm range were used inside a modified UVette adapter (Eppendorf, Hauppauge, NY) with custom optical apertures. The 10 mm pathlength was used for UV-Vis probing based on the molar absorptivities of eosin and the vinyl groups, while the 2 mm pathlength was used for NIR probing, i.e. to allow detection of the low vinyl group concentration from the noise and the broad H_2O bands. H_2O combination bands at 1450 nm and 1950 nm broaden the baseline, as shown in Fig. 1c. The sample volume was 50 μL, which results in sample dimensions of 2 mm × 10 mm × 2.5 mm, where the latter is the thickness in the direction of the excitation light from the LED. At the initial eosin concentrations used, the 2.5 mm depth ensures operation within the thin-film approximation in all experiments. Samples were placed inside a CUV-ALL-UV 4-Way Cuvette Holder (Ocean Optics, Dunedin, FL) with SMA connectors for fiber integration. Fiber optic cables were connected perpendicularly for UV-Vis and FT-NIR analysis at the same z-plane of ~ 1.25 mm (half the depth of the sample).

A fiber optic coupled UV-Vis spectrophotometer (USB4000-FL Miniature Fiber Optic Spectrometer, Ocean Optics, Dunedin, FL) was used to monitor absorbance within the 350–1000 nm range. A UV-Vis-NIR light source was used to emit the probing beam (DH-Mini, Ocean Optics, Dunedin, FL). The UV-Vis probing light was fed into the cuvette holder via a 600 μm solarization resistant fiber optic cable (QP-600-1-SR, Ocean Optics, Dunedin, FL), and a 50 μm receiving fiber optic cable (P50-1-Vis-NIR, Ocean Optics, Dunedin, FL) was connected to the UV-Vis spectrometer. The collimating lens in the cuvette holder and the ~<1 mm diameter pinhole limit the set of incidence angles of the UV-Vis probing beam in this set-up. The acquisition time for the UV-Vis spectrometer was set to ~ 0.5 s (50 ms integration time, 10 scans to average) and a boxcar width of 4 was used. A water reference spectrum was collected prior to every experiment. Eosin-free solutions consisting of PEGDA, VP, and TEA showed no absorption in the UV-Vis region. Only the water peaks overlap slightly with the R-C=C-H NIR band. The UV-Vis probing light was adjusted to the same initial threshold intensity before every experiment.

A fiber optic coupled FT-NIR spectrometer (Nicolet Magna-IR Series II, Thermo Scientific, West Palm Beach, FL) was used to track the vinyl group concentration. FT-NIR spectra were collected with a resolution of 8, a gain of 1, and an optical aperture of 10 with 4 scans at each time point. Acquisition time for the FT-NIR was between 0.5 and 3 s. Two 1000 μm fibers were used to feed the NIR probing light from the spectrometer to the sample, and from the sample back into the InGaAs detector. The FT-NIR spectrometer has a built-in white lamp as probing light source.

A high power fiber coupled multi-wavelength light-emitting diode (LED) light source including a green 500 nm LED (FC8-LED, Prizmatix, Southfield, MI) was used to excite eosin and initiate the polymerization from above the sample. Irradiance (power density) was controlled with a built-in potentiometer and measured with a radiometer (6253, International Light Technologies, Peabody, MA) within the 400–700 nm range. A 3D printed cap was placed on top of the cuvette to restrict the curing light to the sample volume. Negative controls were taken by removal of the initiating 500 nm LED to confirm that the polymerization is not initiated by either the UV-Vis or the NIR probing beams, within the timescale of the polymerization observed with the LED.

Processing of UV-Vis Spectra

As a result of the polymerization reaction, a significant portion of the UV-Vis probing signal is lost due to attenuation by refraction and scattering, as observed in Fig. 2. Hence, for each time point, baselines were fit to 10 points at each end of the wavelength range of interest: 430–650 nm. The absorbance value at the wavelength corresponding to eosin's maximum absorbance (λ_{max}= 523 nm) was then monitored as a function of time, subtracting the time-dependent baseline drift.

In addition, to find the 'kinetically useful' region of the UV-Vis absorbance data, the ratio of the baseline-corrected absorbance at 500 nm to the absorbance at 523 nm (A_{500}/A_{523}) was analyzed. 496 nm is the actual maximum in the LED emission spectrum (see Fig. 2b), but the difference between the intensity at 496 and 500 nm is minimal. When the A_{500}/A_{523} ratio changes substantially, it is an indication that the signal loss from the UV-Vis probing light source is so high that the contamination from the activating LED light (from above) becomes significant. The time point that separates the 'kinetically useful' from the signal-limited data was located by fitting a spline to the ratio as a function of time and then calculating the maximum second derivative. To ensure that the signal loss does not interfere with the measurement of eosin concentration via its absorbance, the end point of the useful regime was determined by finding the maximum of the second derivative of the absorbance at 523 nm and then fitting 80% of the absorbance data between the end of the inhibition period and the second derivative maximum. The maximum second derivative of the absorbance at 523 nm occurs before the change in the ratio of the absorbance at 500 nm and 523 nm. Fitting 80% of the data in this regime serves as an added precaution against inadvertently misinterpreting artifacts resulting from signal loss. Single exponentials were fit to the inhibition periods and the periods immediately following the onset of polymerization.

Processing of FT-NIR Spectra

The vinyl group concentration was determined by integrating the peak area between 6229 and 6128.8 cm^{-1} for the first overtone of the =C-H bond(s) associated with the acrylate group centered at 6180 cm^{-1} (1618 nm) using the built-in function in the OMNIC software.

The inhibition times were determined by first plotting the conversion, defined as $(A_0\text{-}A)/A_0$, as a function of time. The time for which the conversion value remained within the noise level of the FT-NIR detector is considered as the inhibition time, and was determined numerically. The longest time for which a value of 0 was calculated for the conversion was used as the starting point in an iterative fitting procedure, in which second order polynomials were fit to the subsequent 200 data points (~130 seconds). This time was also used as the initial guess to find the root (the inhibition time). This fitting procedure was performed iteratively until the difference between two consecutive roots was < 0.1 seconds. Second order polynomials were used in the fitting procedure in order to balance the effects of noise and nonlinearity. The fitting would otherwise have been restricted to smaller range.

The polymerization rate was determined by differentiating the function generated by fitting a smoothing spline with a smoothing parameter of 1×10^{-5} to the raw conversion data starting at the root, found through the iterative process. The smoothing parameter was selected so that the spline captured trends in the data without capturing the noise (larger values resulted in the spline being fit to signal noise). The resulting derivative was multiplied by the initial vinyl group concentration to give the rate of polymerization (R_p). The intercept of the spline was also calculated and found to agree with the value determined through iteratively fitting a second order polynomial. While differential scanning calorimetry (DSC) gives a more precise quantification of R_p, we are interested in finding R_p trends in response to perturbations, such as the presence of oxygen. The conclusions derived from the trends should hold using the conversion data from the FT-NIR.

Dynamic Photorheology

Dynamic Mechanical Analysis in shear mode was performed in a 4400 Ares Rheometer (TA Instruments, adapted for *in-situ* fiber optic coupled LED photopolymerization experiments). Frequency and strain sweeps were performed for the initial solution and the final hydrogel material to confirm that we are in the viscoelastic region. The storage (elastic) and loss (viscous) moduli were then determined by a dynamic time sweep with an 8 mm diameter plate and a sample thickness of 500 μm at a frequency of 0.5 rad/s and 1% strain. Irradiation with the 500 nm LED at 3.7 mW/cm^2 was performed to match the conditions in the UV-Vis/FT-NIR instrument. It was confirmed that there was no significant evaporation at these conditions through a comparison of the results with those obtained using an oil layer around the sample. A crossover determination was not possible for the formulations at these conditions.

Results and Discussion

In-situ UV-Vis monitoring of hydrogel polymerization

Eosin consumption was measured by monitoring the maximum absorbance peak for the ground state of eosin at 523 nm. This analysis was complicated by attenuation of the UV-Vis signal through the sample during the polymerization. As shown in Fig. 2, the baseline absorbance increases as the polymerization progresses. This is a result of signal loss caused by non-absorptive attenuation, i.e. less probing light reaches the detector with time. Eventually, scattered light from the initiating 500 nm LED creates a dip that coincides its spectral output. An inversion in the absorbance at the peak fluorescence emission wavelength of eosin, 550 nm, also occurs. These effects are caused by time-dependent changes in refraction and scattering from the hydrogel. It is necessary to account for these phenomena in order to extract reliable information about the time-dependent concentration of eosin during the polymerization reaction from the UV-Vis data.

Metrics for quantifying optical attenuation (signal loss)

Non-absorbing processes that attenuate the UV-Vis probing light are scattering, refraction, and reflection.[27] Polymers are known for having a higher refractive index than their precursor monomers; this feature forms the basis for holographic polymer gratings.[32] Using UV-Vis spectroscopy, Schmitt captured changes in refractive index (n) as wavelength-independent shifts in light transmission during the bulk polymerization of 50-μm thick acrylic monomer films (the absorbance baseline increased and decreased before returning to its initial level).[27] Ultimately, these baseline shifts were attributed to time-dependent fluctuations in scattering and refraction arising from density fluctuations and heterogeneities.

While scattering phenomena are diverse and highly complex, we attempt herein to correlate the more understood types of scattering that have been observed for polymer solutions, including PEGDA in water systems: Mie and Rayleigh scattering.[33,34] Mie scattering refers to an analytical solution to Maxwell's equations for a few particle geometries, while Rayleigh scattering is a simplification of the Mie solution for the case when the particle size is much smaller than the wavelength ($\leq 0.1\lambda$).[35] It is noteworthy that λ-independent Mie scattering has a greater forward component (anisotropic) than λ-dependent Rayleigh scattering (isotropic). When we analyzed the baseline shifts for the case of the PEGDA hydrogels, we noticed that the absorbance baseline in the blue light region (~430 nm) increased more steeply than the absorbance baseline at longer wavelengths, e.g. 650 nm (Fig. 2b). This form of wavelength dependence is frequently indicative of Rayleigh scattering, for which the intensity of the scattered light scales with the inverse of λ^{4}.[36] It is known that solutions of PEG oligomers in water can scatter light both with Mie and Rayleigh characteristics, depending on the PEG content and molecular weight.[33]

Furthermore, Small Angle Neutron Scattering (SANS)[37,38] and Brillouin scattering[39] measurements have confirmed that PEG-based hydrogels are heterogenous and rich structures, especially when polymerized via a chain growth mechanism. Lin-Gibson et al. have shown SANS evidence for PEGDMA hydrogels of the formation of mesoscale (1–100

nm) clusters and domains, which are associated with the mechanical robustness of these PEG-based networks.[37,38,40] Hence, it appears that hydrophobic PEGDA-rich domains within the hydrophilic polymer network as well as carbon-based links of a macrogel can fulfill the length-scale requirement for Rayleigh scattering (~40 nm) in the blue-light region.

Consequently, we can utilize a simplified power law expression to separate the more strongly λ-dependent Rayleigh scattering from the relatively λ-independent phenomena (Mie scattering, reflection, and refraction) that together can lead to non-absorbing optical attenuation and baseline shifts as a result. To account for the wavelength independent attenuation as well as the apparent wavelength dependent scattering, the intensity of the transmitted UV-Vis probing light (I) can be expressed as follows:

$$\frac{I}{I_0}=10^{-\mu_T}$$

where I_0 is the incident irradiance and μ_T is the extinction or attenuation coefficient. μ_T can be expressed as the sum of the processes that lead to optical attenuation

$$\mu_T=\mu_S+\mu_R+\mu_r+\mu_A$$

where the subscripts correspond to the coefficients for scattering, refraction, reflection and absorbance, respectively. Since we are dealing with non-absorbing processes, $\mu_A = 0$. This leaves us with the expression:

$$\mu_T=\mu_S+\mu_R+\mu_r$$

Expressing the modified equation in terms of absorbance (as obtained from the spectrophotometer), which in reality is due to non-absorbing optical attenuation, we obtain

$$log_{10}\left(\frac{I_0}{I}\right)=\mu_T=\mu'_S\left(\frac{1}{\lambda^4}\right)+\mu_R+\mu_r$$

where the calculated ‘absorbance’ by the spectrophotometer in the range of wavelengths where no molecules absorb corresponds, in reality, to the μ_T attenuation coefficient with λ-dependent and λ-independent components. In order to deconvolute these two components we express μ_S as $\mu'_S(1/\lambda^4)$, assuming a Rayleigh dependence on wavelength.[35]

In this case, we observe that light transmission decays as a function of time, as opposed to Schmitt’s observations where transmission went through a maximum. This indicates that the anisotropic Mie component from the heterogeneities is negligible, i.e. there is no exclusive increase in forward scattering. Thus, we can lump all λ-independent components into a single term with refraction and reflection, μ'_R.

$$\mu_T = log_{10}\left(\frac{I_0}{I}\right) = \mu'_S\left(\frac{1}{\lambda^4}\right) + \mu'_R$$

Assuming the above dependence on wavelength, baselines were fit to the absorbance spectra using 10 points at each end of the wavelength range of interest: 430–650 nm. This allows for an assessment of the relative contributions of the wavelength independent and dependent signal loss in the form of μ'_S and μ'_R. Fig. 3 shows these coefficients as a function of time for the sample represented in Fig. 2. In order to permit a comparison of the contribution of the two coefficients, μ'_S from the time-dependent baseline fitting was multiplied by the wavelength-averaged $1/\lambda^4$.

Comparing μ'_S and μ'_R in Fig. 3a & b, we first show that neither μ'_S nor μ'_R change during the 43 s of inhibition where no monomer is consumed. After 43 s, only the λ-dependent scattering (μ'_S) increases until 90 s of irradiation, which we propose is due to the very early stages of the polymerization where the slight increase in molecular weight allows for the formation of PEGDA-rich domains in the mesoscale (tens of nanometers).[37,38] Between 90 and 175 s, both μ'_S and μ'_R increase almost linearly with time. However, during this period μ'_R increases from 0 to 0.15, whereas μ'_S increases from 0.02 to 0.04. After 175 s of irradiation, μ'_S increases dramatically until the 235 s mark, where it goes through a maximum. In contrast, μ'_R begins its rapid increase around 200 s.

The contribution from μ'_S (3% of the total optical attenuation) becomes negligible after 300 s of irradiation, as seen in Fig. 3c. This behavior was consistent across all of the samples, under different curing light intensities and purging conditions, and suggests that the sub-40 nm heterogeneities in density and/or refractive index are formed during the first stages of hydrogel formation, and then disappear as the hydrogel homogenizes.

We propose that μ'_S is initially more important because of the formation of nanogels (sub-40 nm). As these nanogels swell and begin to interconnect, they form microgels and, ultimately, a macrogel. Before this macrogel is swollen by the water, its structural features lead to the drastic increase in μ'_S and μ'_R, where μ'_S increases first. Once the macrogel starts to expand as the water molecules permeate the crosslinked structure, these secondary sub-40 nm features composed of carbon-rich linkages (crosslinks) expand to length-scales that are closer in size to the probing wavelengths. Hence, the Rayleigh scattering features essentially disappear, thus leading to a decrease in μ'_S. This suggests that the point where μ'_S goes through its maximum corresponds to the point at which the sub-40 nm heterogeneities are lost due to swelling of the hydrogel and all that remains is a relatively homogenous hydrogel with carbon-rich domains throughout the structure. The differences in the refractive index of these carbon-rich domains (n_{PEG}=1.4590[41], n_{PEGDMA}=1.5063[42]) and the surrounding water (n=1.33[43]) explain the dominant contribution of μ'_R to the final optical attenuation, as shown in Fig. 3. The time at which μ'_S goes through a maximum, for both ambient and purged conditions, decreases as the light intensity increases (Table S1), a result of a higher rate of polymerization (R_p). The conversion where μ'_S is at a maximum was consistently between 0.27 and 0.37 (Table S2) with varying irradiance, further suggesting that the μ'_S maximum is related to macrogelation.

In fact, photorheology experiments (Fig. S3) indicate that the start of the modulus increase (outside the initially noisy torque values) coincides with the start of the development of μ'_R at approximately 100 s, whereas the point in time at which the rate of increase of G′ plateaus coincides with the time where μ'_S goes through a maximum value (~ 253 s). We propose that the correlation between these transitions in mechanical properties and the optical attenuation parameters strongly supports the initial formation of nanogels, the subsequent and slow transition to microgels, and the ultimate accelerated macrogelation, with the final production of a mechanically robust gel with a G′ of around 170 kPa. The buildup in the storage modulus correlates with the increase in μ'_R, as detailed in Fig. S3.

A_{500}/A_{523} ratio as indicator of signal contamination due to scattering

To determine the point at which optical attenuation undermines reliable interpretation of the UV-Vis data, the ratio of the baseline-corrected peak height at 500 nm (the wavelength of the LED curing light) to the peak height at 523 nm (the wavelength at which the eosin absorbance is at a maximum) was tracked. 500 nm was selected as noise from scattered or refracted photons from the initiating LED light becomes significant as the UV-Vis probing light is increasingly attenuated, accounting for the logarithmic nature of the Beer-Lambert law. For example, at 310 s, the baseline at 500 nm is at ~1.5 AU, which translates into only 3% transmission of the initial UV-Vis probing light. Hence, if the scattered light from the initiating LED originally accounted for 1% of the total photons reaching the detector, now it would represent at least 20% of the total photons.

A reduction in the absorbance at 500 nm relative to the absorbance at 523 nm indicates that light from the LED curing light is reaching the detector, altering the characteristic absorbance spectrum for eosin. It is worth noting that as eosin is consumed and the absorbance decreases, some peak broadening is expected and, consequently, a change in the ratio of the absorbance at 500 nm to that at 523 nm. However, peak broadening would have the opposite effect, contributing to a slight increase in the A_{500}/A_{523} ratio. Fig. 3d shows the normalized baseline fitting parameter μ'_S and the ratio of the absorbance at 500 nm to 523 nm. Around 240 seconds, the ratio of the absorbance at 500 nm to the absorbance at 523 nm begins a precipitous descent. This closely follows the μ'_S maximum at 235 seconds. These transition times and the corresponding average vinyl fractional conversions are summarized in Tables S1 and S2. Beyond an average vinyl fractional conversion of 0.3, it is difficult to reliably determine the absorbance at 523 nm resulting from eosin in its ground state. However, it is still possible to draw conclusions from the change in absorbance prior to this transition and this analysis demonstrates the wealth of information contained within the UV-Vis absorbance data, and the significance of being able to correlate this to FT-NIR results.

Correlating eosin consumption with vinyl conversion from FT-NIR

Having established the contribution of non-absorptive attenuation to the absorbance signal and identified the point beyond which initiating LED contamination is observed, we can interpret the absorbance of ground state eosin in the context of the conversion data and identify the regions from which information about eosin consumption can be reliably obtained. The first 43 s during which there is no polymerization (the average vinyl fractional conversion is 0) is the inhibition period (Fig. 3a & b). During this time, the oxygen present

in solution is thought to react with radicals to form peroxy radicals,[44] which are essentially unreactive towards propagation and thus effectively inhibit the polymerization. Before the onset of polymerization, the absorbance at 523 nm decays at a nearly imperceptible rate (Fig. 4a). Once the oxygen in the system has been depleted, the polymerization begins and the maximum rate is attained immediately. The absorbance at 523 nm begins to decay more rapidly with the onset of polymerization. As the polymerization proceeds and the double bond conversion increases, the rate of polymerization slows (Fig. S1). This rate reduction occurs as the polymer cross-links and a network forms, slightly slowing the diffusion of the monomers and propagating radicals into and out from the PEGDA-rich domains.

After 240 s of irradiation, the rate of absorbance decay increases further. As shown in Fig. 2, at this point in the polymerization, an increase in the optical attenuation and significant noise from the initiating LED are evident. This transition corresponds closely with the maximum in the wavelength-dependent parameter μ'_S, which occurs at 235 s, further supporting the homogenization of the macrogel as the water permeates and the hydrophobic pockets become more uniformly distributed, as depicted in the islets of Fig. 2.

Analysis of eosin photobleaching kinetics as a function of vinyl conversion

As previously noted, the rate of absorbance decay accelerates with the onset of polymerization. As shown in Fig. 4, this acceleration was captured quantitatively by fitting single exponentials to the inhibition period (region 1) and the period immediately following the onset of the polymerization (region 2), but prior to the initiating LED contamination and the sharp increase in the baseline absorbance (region 3). The single exponentials are shown in red and cyan for regions 1 and 2, respectively.

For the representative sample shown throughout, the exponential decay constants during the inhibition period (the first 43 s) and the initial polymerization are, respectively 2.3 (± 0.3) × 10^{-4} s^{-1} and 8.5 (± 0.05) × 10^{-4} s^{-1}. The rate of decay increases 3.8x with the onset of polymerization.

The decay constants increase with light intensity for both the inhibition period and initial polymerization period under ambient and argon-purged conditions (Fig. S2). As more light reaches the sample, more of the eosin is excited from its ground state to its singlet state. From its singlet state, eosin can relax back to its ground state or undergo intersystem crossing to its triplet state. Once in its triplet state, eosin can react with itself, oxygen, or TEA. The exchange of an electron and proton with TEA produces the semiquinone form of eosin and a TEA radical, which can react with a monomer to initiate polymerization or react with oxygen to form a peroxy radical. Increasing the light intensity increases the rate at which eosin is excited and consequently the rates of the subsequent reactions. Thus, more of the eosin is irreversibly photobleached as it is consumed in termination reactions that convert it to its leuco form.

The onset of polymerization also has the effect of increasing the decay constant (Fig. S2). The decay constants for the initial polymerization are between 3.0–6.3x greater than those for the inhibition period. At a curing light intensity of 1.5 mW/cm^2, the increase is most pronounced with the polymerization decay constant 5.5x higher than the inhibition period

decay constant. As the curing light intensity is increased to 3.7, 6.0, and 9.6 mW/cm^2, the decay constant increases by a factor of 4.5, 3.7 and 3.0, respectively, with the onset of polymerization.

For the two higher curing light intensities (6.0 and 9.6 mW/cm^2), the average decay constant for the polymerization under argon-purged conditions is 1.3–2.1x higher than under ambient conditions, whereas at the other curing light intensities used, the polymerization decay constants for ambient and purged conditions were similar.

Analysis of the effect of O_2: inhibition time and eosin photobleaching

The experiments performed under ambient conditions were conducted in open vessels, permitting the diffusion of oxygen into the solution, although, as the polymerization progresses and the hydrogel forms, the rate of oxygen diffusion slows. The initial concentration of dissolved oxygen should be close to 0.5 mM, the equilibrium concentration in water; this is 100x greater than the concentration of eosin. For polymerization to occur, the oxygen concentration must be decreased to a level at which radical propagation reactions are favored over inhibition reactions. Independent of the curing light intensity, the absorbance decreases by 1% during the inhibition period. The consistency of this decrease reflects how the oxygen concentration must be reduced below a threshold level for the polymerization to proceed.

The slower rate of absorbance decay during the inhibition period suggests that ground state eosin is being regenerated in the presence of oxygen. In addition, the less rapid decay of the eosin absorbance with the onset of polymerization under ambient conditions relative to purged conditions is likely a consequence of the replenishment of oxygen by diffusion as it is consumed (the oxygen rate of diffusion takes tens of seconds based on the dimensions of the sample and the oxygen diffusivity coefficient in water).[45] This effect becomes more apparent as the light intensity is increased and the initiation rate and rate of oxygen consumption increase.

Slower rates of fluorescence decay have been associated with dye regeneration.[19] Xanthene dyes, such as eosin, are well known oxygen sensitizers. Oxygen has been reported to react with the triplet state of eosin with a rate constant of 1.1×10^9 M^{-1}s^{-1}.[46] The two most commonly presented reactions between triplet eosin and oxygen are as follows:[47]

$$EO^{3*}+O_2 \rightarrow EO^{\cdot+}+O_2^{\cdot-}$$
$$EO^{3*}+O_2 \rightarrow EO+{}^1O_2$$

Of these, the second is considered to be the predominant reaction with a rate constant at least two orders of magnitude greater than the first reaction.[48] This is one pathway through which ground state eosin can be regenerated by oxygen. However, Avens & Bowman have presented an alternative route through which eosin can be regenerated:[10]

$$E^{3*} + TEA \rightarrow EH^{\cdot} + TEA^{\cdot}$$
$$R^{\cdot} + O_2 \rightarrow ROO^{\cdot}$$
$$E\mathrm{H}^{\cdot} + ROO^{\cdot} \rightarrow ROOH + E$$

According to this mechanism, the semiquinone eosin (*EH*˙) resulting from the reaction with TEA is susceptible to hydrogen abstraction by the peroxy radicals (*ROO*˙) that result from the reaction of an initiating TEA radical or propagating radical (here, presented as *R*˙) with oxygen. This regenerates the ground state eosin. Whether this reaction or the reaction that produces singlet oxygen is primarily responsible for the regeneration of eosin depends on the relative concentrations of TEA and oxygen as well as the rate constants for the reactions between the triplet state of eosin and oxygen and TEA. The initial concentration of TEA is 210 mM, 700x the concentration of oxygen. Thus, the probability of a triplet eosin encountering TEA is higher. However, the rate constant for the reaction between triplet eosin and oxygen is reported to be at least two orders of magnitude higher than that between triplet eosin and TEA,[46,47] which means that these reactions occur at comparable rates and likely both contribute to oxygen regeneration. This would be consistent with Avens & Bowman's suggestion that additional regeneration pathways available to eosin in the presence of oxygen, beyond the peroxy radical hydrogen abstraction, may account for its ability to overcome 1000-fold excess oxygen as compared with only 100-fold excess 2,2,6,6-tetramethyl-1-piperidinyloxy (TEMPO) inhibitor.[10]

Fig. 4b shows the dependence of the inhibition time on the intensity of the initiating LED. The linear dependence (slope=−1.07 ± 0.5, R^2=0.98) indicates the oxygen is consumed in a nonchain process, i.e. that each initiating radical consumes only one oxygen molecule.[49] This is notable as it implies that TEA is not serving as a hydrogen donor to peroxy radicals. Due to their reactivity as hydrogen donors, amines, and in particular tertiary amines such as TEA, are used as additives to suppress oxygen inhibition.[12] In spite of the excess of TEA relative to eosin, this analysis suggests that hydrogen donation from TEA does not lead to reinitiation of the polymerization, which further implies that hydrogen abstraction processes, such as the reaction between peroxy radicals and the semiquinone form of eosin, are not the primary pathway through which oxygen inhibition is overcome.

Conclusions

Dual UV-Vis/FT-NIR monitoring allows for simultaneous monitoring of chromophore (initiator) and monomer reactive group concentrations. Here, we applied this tool to the study of the eosin-activated photopolymerization of PEGDA hydrogels. Contributions from non-absorptive processes in addition to the absorptive processes of interest in this study added a degree of complexity to proper interpretation of the spectral data. We presented a strategy for quantifying signal loss associated with microgelation and network formation, accounting for both wavelength-dependent and wavelength-independent light attenuating processes and introducing metrics for monitoring the extent of signal loss: a wavelength-dependent baseline fitting parameter, μ'_S, and the ratio of the absorbance at the wavelength of the initiating LED to the peak absorbance of the photoinitiator. The values of these metrics changed markedly when the average vinyl fractional conversion was between 0.3

and 0.4, indicating macrogelation. Practically, these metrics were used to establish an upper bound for the reliability of the absorbance data. Having established a method for treating the data, we demonstrated how the coupled technique could be used effectively to investigate oxygen inhibition and dye regeneration. We showed that the consumption of eosin increases by a factor of 3 or more following the inhibition period, a finding consistent with previous reports of eosin regeneration by oxygen. Finally, we present evidence suggesting that hydrogen abstraction from TEA or the semiquinone form of eosin by peroxy radicals does not explain the unusual reactivity of the system described here in the presence of oxygen.

As an added benefit, the method of deconvoluting Uv-vis signals arising from absorptive and non-absorptive processes also provided information about the time-dependent structural richness of the hydrogel as it formed. The underlying principles of the signal loss quantification method are generally applicable. This method could be applied to different chromophores with appropriate modifications to the wavelength of interest to analyze the dynamic morphology of a wide range of polymer networks.

Supplementary Material

Refer to Web version on PubMed Central for supplementary material.

Acknowledgments

A National Science Foundation Graduate Research Fellowship (to K.K.), a Burroughs Wellcome Fund Career Award at the Scientific Interface (to H.D.S.) and the Department of Defense (Congressionally Directed Medical Research Program, Prostate Cancer Research Program Award No. W81XWH-13-1-0272) supported this work. The opinions, interpretations, conclusions, and recommendations are those of the authors and are not necessarily endorsed by the Department of Defense. NIH/NIDCR R01DE014227, the NSF Industry/University Cooperative Research Center for Fundamentals and Applications of Photopolymerization, and CONACYT (Consejo Nacional de Ciencia y Tecnología) 308269 supported the building of the coupled NIR/UV-vis spectroscopy apparatus.

References

1. Fouassier J, Allonas X, Burget D. Prog Org Coatings. 2003; 47:16–36.
2. Yagci Y, Jockusch S, Turro NJ. Macromolecules. 2010; 43:6245–6260.
3. Scott TF, Kowalski BA, Sullivan AC, Bowman CN, McLeod RR. Science (80-). 2009; 324:913–917.
4. Rengier F, Mehndiratta A, Tengg-Kobligk H, Zechmann CM, Unterhinninghofen R, Kauczor HU, Giesel FL. Int J Comput Assist Radiol Surg. 2010; 5:335–341. [PubMed: 20467825]
5. Cruise GM, Hegre OD, Scharp DS, Hubbell JA. Biotechnol Bioeng. 1998; 57:655–65. [PubMed: 10099245]
6. Cruise GM, Scharp DS, Hubbell JA. Biomaterials. 1998; 19:1287–94. [PubMed: 9720892]
7. Hansen RR, Sikes HD, Bowman CN. Biomacromolecules. 2008; 9:355–62. [PubMed: 18052028]
8. Kaastrup K, Sikes HD. Lab Chip. 2012; 12:4055–4058. [PubMed: 22930231]
9. Badu-Tawiah AK, Lathwal S, Kaastrup K, Al-Sayah M, Christodouleas DC, Smith BS, Whitesides GM, Sikes HD. Lab Chip. 2015; 15:655–659. [PubMed: 25427131]
10. Avens HJ, Bowman CN. J Polym Sci Part A Polym Chem. 2009; 47:6083–6094.
11. Bowman CN, Kloxin CJ. AIChE J. 2008; 54:2775–2795.
12. Ligon SC, Husár B, Wutzel H, Holman R, Liska R. Chem Rev. 2014; 114:577–589.
13. Chesneau E, Fouassier JP. Die Angew Makromol Chemie. 1985; 135:41–64.
14. Wong J, Kaastrup K, Aguirre-Soto A, Sikes HD. Polymer (Guildf). 2015; 69:169–177.
15. Shen J, Tian Y, Zeng Y, Qiu Z. Macromol Rapid Commun. 1987; 8:615–620.

16. Decker C, Moussa K. Macromol Chem Phys. 1988; 189:2381–2394.
17. Decker C, Moussa K. Macromolecules. 1989; 22:4455–4462.
18. Cook WD, Chen F. Polym Chem. 2015; 6:1325–1338.
19. Sirovatka Padon K, Scranton AB. J Polym Sci Part A Polym Chem. 2000; 38:3336–3346.
20. Alakhras F, Holze R. Synth Met. 2007; 157:109–119.
21. Decker C. J Polym Sci Part A Polym Chem. 1992; 30:913–928.
22. Chen B, Chrambach A. J Biochem Biophys Methods. 1979; 1:105–116. [PubMed: 551105]
23. Yang DB, Wolf D, Wakamatsu T, Holmes M. J Adhes Sci Technol. 1995; 9:1369–1379.
24. Darcos V, Monge S, Haddleton DM. J Polym Sci Part A Polym Chem. 2004; 42:4933–4940.
25. Gulari E, Mckeigue K, Ng KYS. Macromol Theory Simulations. 1984; 17:1822–1825.
26. Yang DB. J Polym Sci Part A Polym Chem. 1993; 31:199–208.
27. Schmitt M. Macromol Chem Phys. 2011; 212:1276–1283.
28. Kang X, Yu Y, Bao Y, Cai W, Cui S. Polym Chem. 2015; 6:4252–4257.
29. Florenzano FH, Strelitzki R, Reed WF. Macromolecules. 1998; 31:7226–7238.
30. Giz A, Çatalgil-Giz H, Alb A, Brousseau JL, Reed WF. Macromolecules. 2001; 34:1180–1191.
31. Aguirre-Soto A, Hwang AT, Glugla D, Wydra JW, McLeod RR, Bowman CN, Stansbury JW. Macromolecules. 2015; 48:6781–6790.
32. Ke C, Jian-Qun C, Yan W, Ming-Ju H. Chinese Phys B. 2010; 19:014204–8.
33. Liu N, Liu H, Zhu S, Giessen H. Nat Photonics. 2009; 3:157–162.
34. Adam M, Delsanti M. Macromolecules. 1977; 10:1229–1237.
35. Schärtl, W. Light Scattering from Polymer Solutions and Nanoparticle Dispersions. 1. Springer; Berlin/Heidelberg: 2007.
36. Kerker, M. The Scattering of Light and Other Electromagnetic Radiation. Academic Press, Inc; New York, NY: 1969.
37. Lin-Gibson S, Jones RL, Washburn NR, Horkay F. Macromolecules. 2004; 38:2897–2902.
38. Lin-Gibson, Sheng; Bencherif, Sidi; Antonucci, Joseph M.; Jones, Ronald L.; Horkay, F. Macromol Symp. 2005; 227:243–254.
39. Pochylski M, Aliotta F, Blaszczak Z, Gapiński J. J Phys Chem B. 2006; 110:20533–20539. [PubMed: 17034240]
40. Lin-Gibson S, Bencherif S, Cooper JA, Wetzel SJ, Antonucci JM, Vogel BM, Horkay F, Washburn NR. Biomacromolecules. 2004; 5:1280–7. [PubMed: 15244441]
41. Li Q, Zhou H, Hoyle CE. Polymer (Guildf). 2009; 50:2237–2245.
42. Ge J, Goebl J, He L, Lu Z, Yin Y. Adv Mater. 2009; 21:4259–4264.
43. Thormaehlen I, Straub J, Griguli U. J Phys Chem Ref Data. 1985; 14:933–1945.
44. Odian, G. Principles of Polymerization. Wiley Interscience; 2004.
45. St-Denis CE, Fell CJD. Can J Chem Eng. 1971; 49:885.
46. Fouassier JP, Chesneau E. Macromol Chem Phys. 1991; 192:245–260.
47. Neckers, DC.; Valdes-Aguilera, OM. Advances in Photochemistry. Volman, DH.; Hammond, GS.; Neckers, DC., editors. Vol. 18. John Wiley & Sons, Inc; 1993. p. 315-394.
48. Natera JE, Massad WA, Amat-Guerri F, García NA. J Photochem Photobiol A Chem. 2011; 220:25–30.
49. Decker C, Jenkins AD. Macromolecules. 1985; 18:1241–1244.

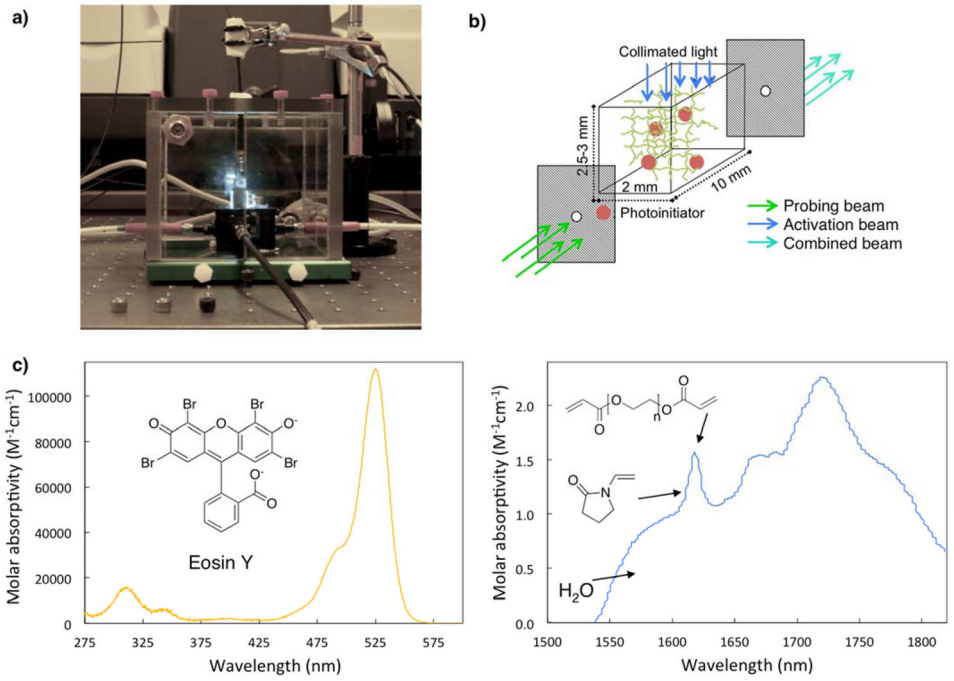

Fig. 1.

a) Photograph of fiber optic coupled UV-Vis/FT-NIR set-up for simultaneous monitoring of μM concentrations of eosin and mM concentrations of vinyl group concentration from poly(ethylene glycol) diacrylate M_n 575 (PEGDA) and 1-vinyl-2-pyrrolidone (VP). Activating light from a green LED (λ_{max} = 496 nm) is shone from above and the entire set-up is encased within an air-excluding case to enable nitrogen-purged polymerization reactions. b) Schematic of polymerizing sample inside a cuvette. Pinholes are used to limit the set of incidence angles of the UV-Vis probing light and restrict the amount of scattered light to the detector. c) UV-Vis absorbance spectrum of eosin (4 μM) and FT-NIR spectrum of PEGDA (420 mM) and VP (35 mM) in water obtained simultaneously.

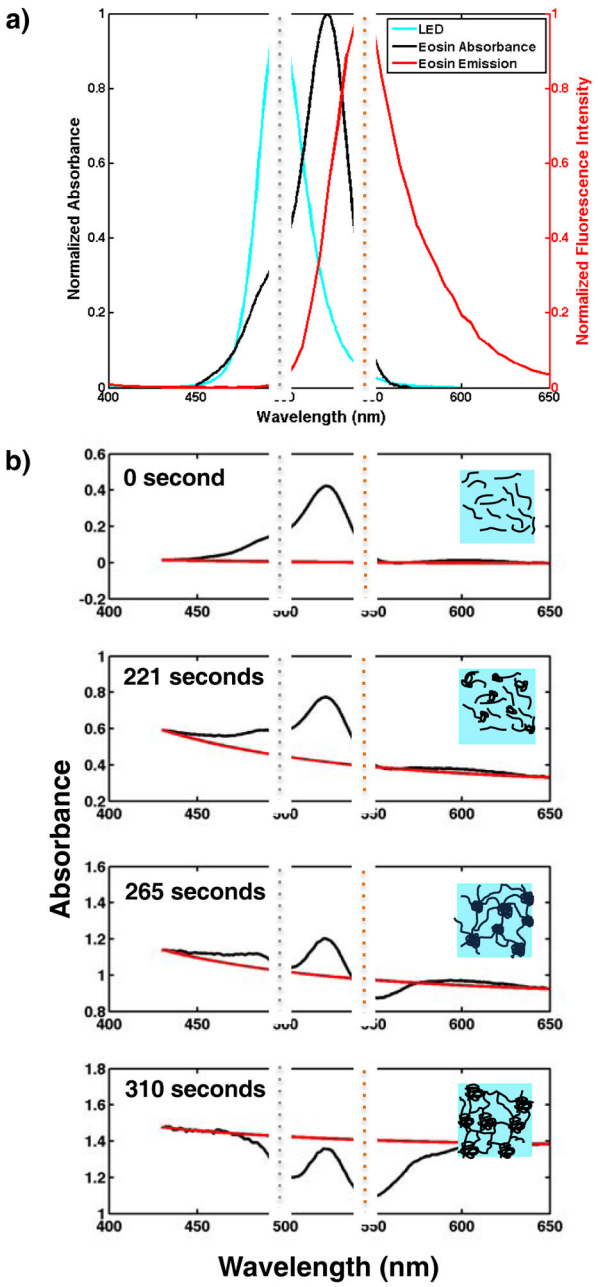

Fig. 2.

a) Eosin absorbance spectra, emission of the initiating LED, and the eosin fluorescence emission spectrum for an aqueous solution consisting of 420 mM PEGDA, 35 mM VP, 210 mM TEA, and 5 μM eosin Y irradiated with a 500 nm LED (3.7 mW/cm^2) under ambient conditions. b) Time-dependent UV-Vis signal loss with baseline shifting and signal contamination from the initiating LED and fluorescence emission. The signal loss is due to non-absorptive optical attenuation from changes in refractive index and scattering as the hydrogels form. This translates into a reduction of the signal-to-noise ratio that leads to the formation of the dips coinciding with the maximum of the LED and the eosin fluorescence emission spectrum.

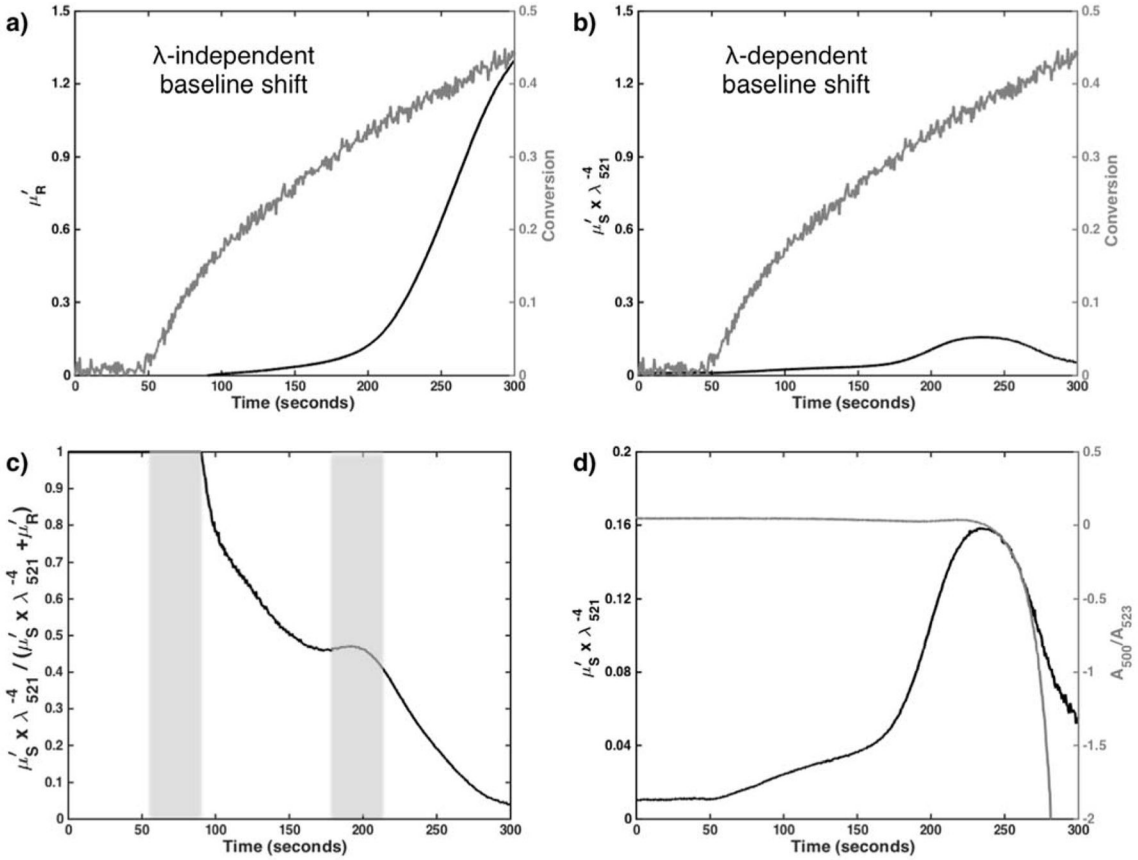

Fig. 3.

Baseline fitting parameters for a solution of eosin, TEA, PEGDA, and VP illuminated with 500 nm light (3.7 mW/cm^2). a) Baseline fitting parameter, μ'_R, representing wavelength-independent light attenuation processes shown in black and average vinyl fractional conversion in gray. b) Baseline fitting parameter, μ'_S, representing wavelength-dependent light scatter and normalized by the average of $1/\lambda^4$ ($1/521\text{nm}^4$), shown in black and average vinyl fractional conversion in gray. c) The fraction of light attenuating processes represented by wavelength-dependent light scattering as a function of time. The sections shaded in gray correspond roughly to nanogelation (left) and macrogelation (right) as supported by photorheology (SI). d) The normalized baseline fitting parameter, μ'_S, shown on a smaller scale in black and the ratio of the absorbance at 500 nm to the absorbance of 523 nm. μ'_S passes through a maximum concurrently with the rapid decline in the ratio.

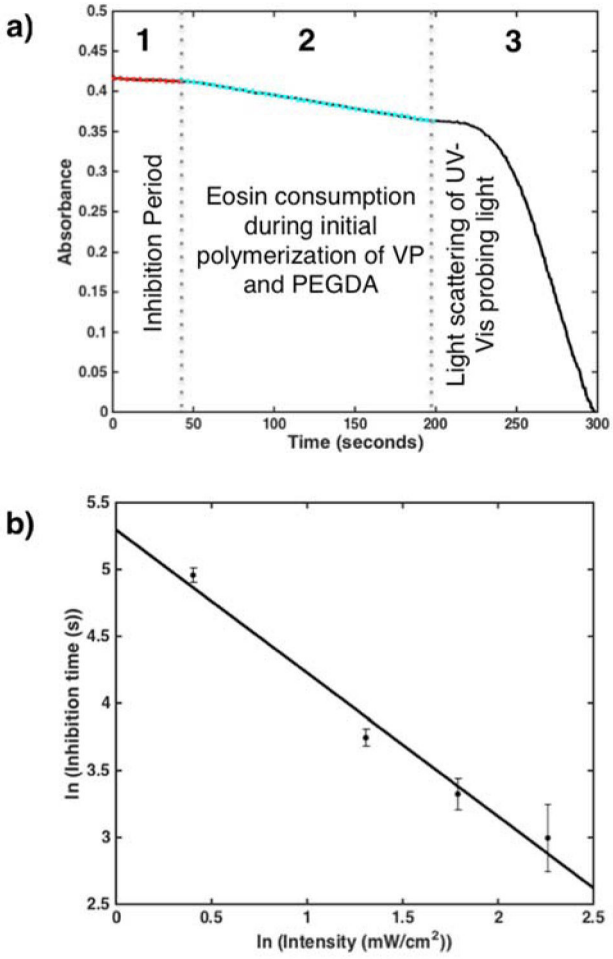

Fig. 4.

a) Single exponentials (dashed lines) were fit to the inhibition period (region 1-red) and to the period immediately following the onset of polymerization (region 2-cyan) for a solution of eosin, TEA, PEGDA, and VP illuminated with 500 nm light (3.7 mW/cm^2) under ambient conditions. The black curve is the baseline-corrected absorbance at 523 nm. b) The inhibition time has a linear dependence on irradiance, indicating the absence of chain peroxidation. Between three and five replicates were performed at each condition.